MODELLING AND ASSESSING IMPACT DAMAGE FOR A NEW GENERATION OF ZERO-EMISSIONS COMPOSITE MARITIME VESSELS

Scott L.J. Millen [1], Emer McAleavy [2], Zahur Ullah [1] and Brian G. Falzon [1,3]

[1] Advanced Composites Research Group (ACRG), School of Mechanical and Aerospace Engineering, Queen's University Belfast, Belfast, Northern Ireland (scott.millen@qub.ac.uk, z.ullah@qub.ac.uk)
[2] Artemis Technologies Limited, Unit 1 Oakbank, Queens Road, Belfast, BT3 9DT (emer.mcaleavy@artemistechnologies.co.uk)
[3] School of Engineering, STEM College, RMIT University, Melbourne, VIC, 3001, Australia (brian.falzon@rmit.edu.au)

Keywords: Impact behaviour, Finite element analysis (FEA), Damage mechanics

ABSTRACT

This paper presents a study of the impact resistance of different composite structures which have been proposed for a new generation of zero-emissions composite maritime vessels. A mixture of flat plate specimens, eFoil leading edge models and full-scale vessel hull models were simulated in this work. These representative models are further divided into high-fidelity models (i.e. mesoscale level of analysis) and global-local finite element (FE) models of the entire structure. Impact conditions were defined based on typical loading expected during the vessels operating life. For example, the leading edge was impacted by sea ice while the hull was impacted by rigid debris. A robust intralaminar damage model was used to capture damage modes such as matrix cracking while cohesive surfaces were used to model ply-to-ply contact and capture delamination.

Results have shown that the leading edge can successfully resist an ice impact with negligible predicted interlaminar delamination when compared with a rigid body impact. The use of a global-local modelling approach (a mixture of shell and solid elements and shell-solid coupling) can produce similar damage in local and global representations of the eFoil structure. Results have also shown that, when a projectile strikes the hull, interlaminar delamination was negligible.

1 INTRODUCTION

The growing global mandate to cut CO_2 emissions from all modes of transport is driving significant innovation within the maritime sector. The International Maritime Organisation (IMO) has proposed that the global maritime sector should cut emissions by at least half by 2050 [1]. Recently, new maritime designs, derived from aerospace and motorsport have been proposed to aid in the decarbonisation of the maritime industry. The use of hydrofoils, wing-like structures under the vessel which lift the hull out of the water, can produce an order of magnitude reduction in wetted area and drag [2]. Composite eFoils are an evolution of hydrofoils, which not only make use of lightweight materials but also integrate an electric drivetrain and control surfaces.

The susceptibility of in-service damage to the vessel varies above and below the waterline and each needs to be reliably assessed. eFoils may be damaged in the presence of debris, by striking large marine life, or during production and servicing. Above the waterline, the vessel can additionally sustain hull damage through collision with other vessels or when docking.

A thorough assessment of the different damage scenarios, extent of damage, and influence on operation would require extensive, costly and time-consuming physical testing. Therefore, simulations can be used to predict the likely complex interacting failure modes, during impact, in carbon fibre reinforced polymer (CFRP) composites, whether used in monolithic or sandwich construction.

A large number of experimental and numerical studies have been undertaken to represent low velocity impact (LVI) and compression after impact (CAI) testing on CFRP [3–6]. Within maritime research, a number of works have focussed on the failure of composites due to impact from ice [7,8] and slamming impact [9] on the hull. However, the majority of preceding LVI studies have used specimens with dimensions suitable for drop-tower impact experiments (150 mm x 100 mm) and do not represent the entire aircraft or vessel structure. Recently, a number of works have used different multi-scale modelling methods to simulate damage, due to impact or other loading conditions, on composite structures [10–15].

The aim of this work is to assess the influence of in-service damage on operability. In particular, LVI damage arising from submerged debris. Therefore, a number of models were developed to assess the likely impact damage and resulting reduction in CAI strength. A well established intralaminar damage model was used to simulate damage at the ply level. A mixture of mesoscale and multi-scale models were used in this study.

2 METHODOLOGY

2.1 Intralaminar Damage Model

An in-house VUMAT subroutine, for ABAQUS/Explicit [16], was used to model intralaminar damage [3,17–21]. This damage model can capture both fibre-dominated and matrix-dominated damage and load reversal. It has an advanced characteristic length calculation ($l_{fib} = V_0^e/A_e$, where V_0^e is the undeformed volume of the element, and A_e is the fracture surface area) found using an approach proposed by Chiu et al. [22] based on a search algorithm which maximises damage initiation functions. A non-linear shear model with kinematic hardening for the matrix [23]; and robust element deletion control (if $d_{11} > 0.99$, or $det\boldsymbol{F} < 0.1 \vee det\boldsymbol{F} > 3.0$ where $det\boldsymbol{F}$, which is available as an internal argument passed to the VUMAT subroutine from ABAQUS/Explicit, yields the ratio of the deformed volume, V^e, to the undeformed volume, V_0^e), for CAI and composite crushing modelling, were also used.

Linear elasticity is assumed up to failure in the longitudinal and transverse directions with an inelastic response in shear. A quadratic strain-based failure criterion was used to model tensile and compressive damage initiation in the longitudinal direction:

$$F_{11}^{t(c)} = \left(\frac{\varepsilon_{11}}{\varepsilon_{11}^{0t(c)}}\right)^2 \tag{1}$$

where $F_{11}^{t(c)}$ are the failure indices for tension and compression, respectively, $\varepsilon_{11}^{0t(c)}$ is the tensile/compressive fibre failure initiation strain and ε_{11} is the current fibre strain. Transverse matrix-dominated damage initiation was captured using the criterion proposed by Catalanotti et al. [24]:

$$F_{mat} = \left(\frac{\sigma_{NN}}{S_{23}^{is}}\right)^2 + \left(\frac{\sigma_{NT}}{S_{23}^{is}}\right)^2 + \left(\frac{\sigma_{NL}}{S_{12}^{is}}\right)^2 + \lambda\left(\frac{\sigma_{NN}}{S_{23}^{is}}\right)\left(\frac{\sigma_{NL}}{S_{12}^{is}}\right)^2 + \varkappa\left(\frac{\sigma_{NN}}{S_{23}^{is}}\right) \text{ for } \sigma_{NN} > 0, \tag{2}$$

$$F_{mat} = \left(\frac{\sigma_{NT}}{S_{23}^{is} - \mu_{NT}\sigma_{NN}}\right)^2 + \left(\frac{\sigma_{NL}}{S_{12}^{is} - \mu_{NL}}\sigma_{NN}\right)^2 \text{ for } \sigma_{NN} < 0. \tag{3}$$

where F_{mat} is the failure index for matrix tensile and compressive failure, and σ_{ij} (i, j = N, T, L) are the stresses acting on the fracture surface. Parameters κ and λ are defined by $\lambda = 2\mu_{NL}\, S_{23}^{is}/S_{12}^{is} - \kappa$, and $\kappa = \left(\left(S_{12}^{is}\right)^2 - \left(Y^{t,is}\right)^2\right)/\left(S_{23}^{is} Y^{t,is}\right)$, where S_{12}^{is} and S_{23}^{is} are the in-situ in-plane and out-of-plane shear strengths, respectively. The transverse friction coefficients, μ_{NT} and μ_{NL}, are defined based on Mohr-Coulomb's theory. $Y^{t,is}$ and $Y^{c,is}$ are the in-situ transverse tensile and compressive strength, respectively.

Through-thickness matrix-dominated damage initiation was controlled by the modified Hashin criterion [25], which considered the interaction between normal stress (σ_{33}) and shear stress (τ_{13} and τ_{23}) on the plane perpendicular to the through-thickness direction:

$$F_{33}^{t} = \left(\frac{\sigma_{33}}{\sigma_{33}^{0t}}\right)^2 + \left(\frac{\tau_{13}}{\tau_{13}^{0t}}\right)^2 + \left(\frac{\tau_{23}}{\tau_{23}^{0t}}\right)^2 - 1 \geq 0, \sigma_{33} \geq 0, \quad (4)$$

$$F_{33}^{c} = \left(\frac{\sigma_{33}}{\sigma_{33}^{0c}}\right)^2 + \left(\frac{\tau_{13}}{\tau_{13}^{0c}}\right)^2 + \left(\frac{\tau_{23}}{\tau_{23}^{0c}}\right)^2 - 1 \geq 0, \sigma_{33} < 0, \quad (5)$$

This intralaminar damage model has been used extensively for LVI/CAI modelling and more details about the model and validation can be found in refs. [3,17–21]. Cohesive surfaces were used to model ply-to-ply contact and capture delamination using a bilinear traction-separation law.

2.2 Impact Specimens

Three types of simulations were used in this work; flat plate specimens, following established test standards developed for the aerospace sector [26], eFoil leading edge models and full vessel hull models, both based on representative geometry from industrial partners, Artemis Technologies Ltd. These representative models are further divided into high-fidelity models (i.e. mesoscale level of analysis) and global-local finite element (FE) models of the entire structure. Therefore, four models are discussed in this work.

eFoil Simulations

Firstly, local high-fidelity simulations were used to predict the behaviour of eFoil structures under impact. This model, shown in Figure 1a, was built from representative geometry and featured the leading edge (blue), reinforcement (white), and core (green). The foil section measured 150 mm in length and represented a section extracted from the centre of the full leading edge. A rigid support fixture was also used in this model to support the leading edge, approximating the support offered by a spar section. 68,564 linear hexahedral elements of type C3D8R were used on the leading edge.

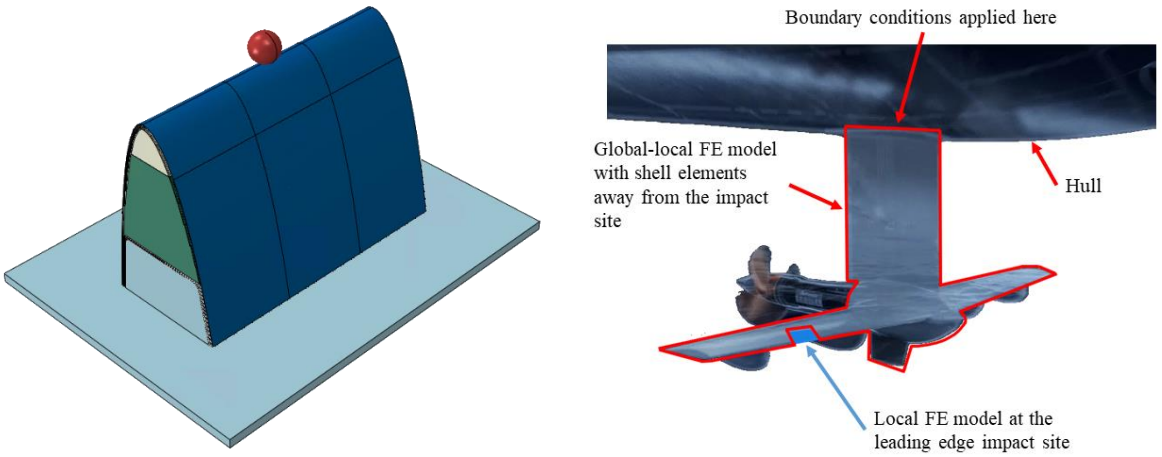

a) eFoil mesoscale model b) eFoil global-local model

Figure 1: a) eFoil mesoscale model and b) eFoil global-local model.

This model was then embedded in a global-local FE representation of the entire foil structure, shown in Figure 1b. This modelling approach was used to simplify the representation of additional components, away from the impact site, using shell elements [10]. A mixture of continuum shell 3D 8 nodal elements (SC8R), planar shell 3D 4 nodal elements (S4R) and two-dimensional shell elements (S3R) were used

to achieve the FE mesh. A total of 106,816 elements, of which 38,252 were shells, were used in the global-local eFoil model. A full breakdown of the elements used in both models is given in Figure 2.

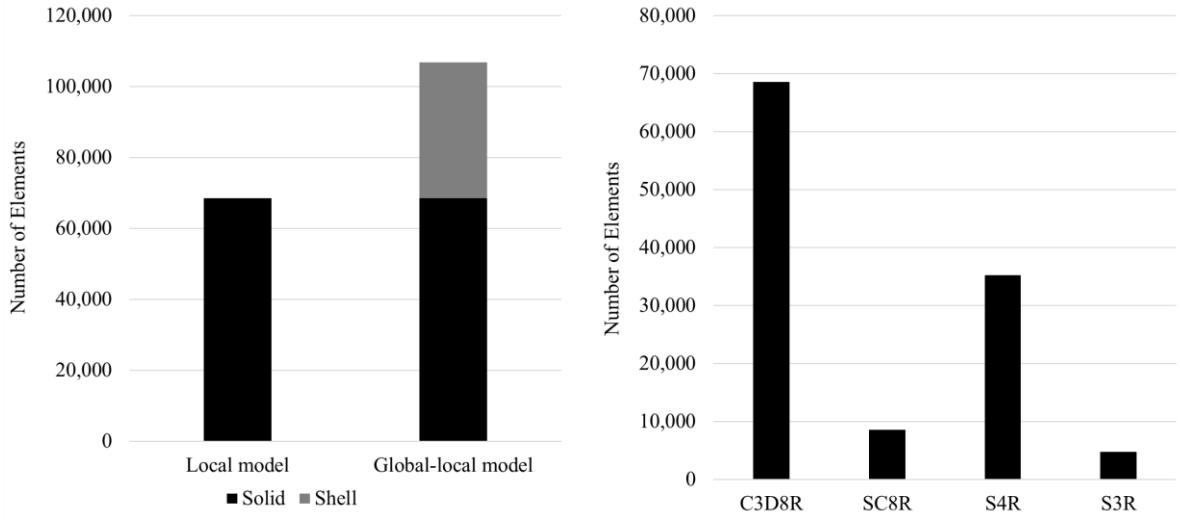

a) Comparison of element count between models

b) Breakdown of element types in global-local model

Figure 2: Summary of elements used in eFoil local and global-local models

Two types of impactors were used in both cases. Firstly, a rigid impactor, modelled as a spherically shaped rigid surface, with a 2 kg lumped mass assigned to a reference point. The second type was a block of ice, which represented a potential "event-based" load case during operation. Since the vessel would not operate in extremely icy conditions the block of ice was kept small in terms of geometry and mass. Therefore, a small block measuring 35 mm x 40 mm x 40 mm was used. The material model for ice was derived from the work of Liu et al. [27] which included strain rate effects. The density of the ice was 900 kg/m^3, the Young's modulus was 9.38 GPa and the tensile strength was 0.517 MPa. The resulting mass of the ice block was 0.05 kg. Given the difference in mass between this ice block and the rigid impactor, a further simulation was completed in which the density of ice was modified to a target mass of 1 kg. The strain rate-dependent material model for ice was coupled with the SPH (Smoothed Particle Hydrodynamics) method [28] to accommodate the large deformation of the ice on impact.

The velocity of the rigid impactor was 10 knots (5 m/s) which resulted in an impact energy of 25J. The velocity of the ice block was 34 knots (17.5 m/s), the top speed of the vessel.

Hull Simulations

The hull was also represented using two models, shown in Figure 3. Initially, a 150 mm x 100 mm flat hull model was created which was assumed to be a small sub-section of the hull and therefore had no curvature. This specimen was supported by a picture frame with an inner unsupported region of 75 mm x 125 mm. The material system and layup for the hull structure was a quasi-isotropic sandwich structure with a mixture of woven and cross-ply carbon fibre. The nonlinear behaviour of the foam core was modelled using the crushable foam plasticity model with volumetric hardening available in ABAQUS through the CRUSHABLE FOAM and CRUSHABLE FOAM HARDENING options. The hardening behaviour was represented using a uniaxial compressive stress versus plastic strain relationship [29]. 65,280 C3D8R hex elements were used for the hull model with ten elements through the thickness of the core. In this case, the impact velocity was 10 knots (5 m/s), representing an impact while docking, since it was unlikely that the hull would collide with debris during foiling at the top speed of the vessel.

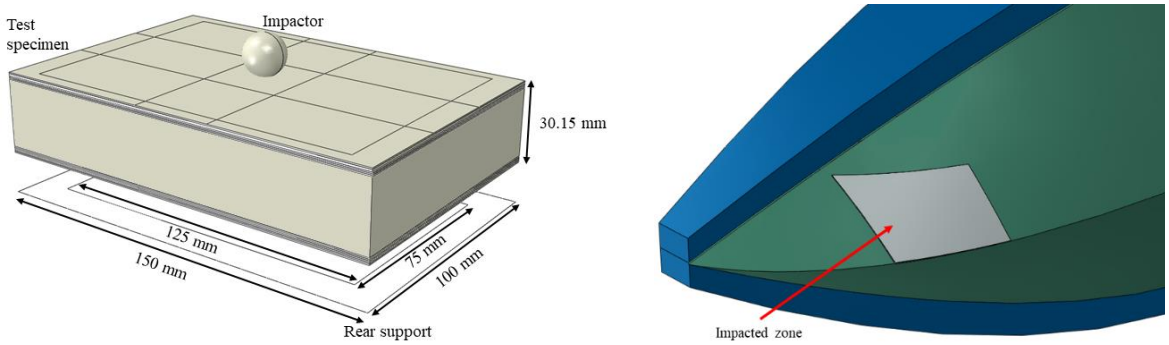

a) Flat hull representation b) Global-local hull model

Figure 3: Different hull model representations

A larger global-local model of the entire hull structure under representative loading, accounting for curvature, was also created, Figure 3b. A similar approach to the global-local model of the eFoil was used here with both solid (the local region under impact) and shell regions linked with shell-solid coupling, shown in Figure 4. Additional reinforcement in the hull was included and was connected to the main body of the hull using tie constraints. As before a spherical, rigid impactor was used with a velocity of 10 knots (5 m/s).

The mesh was refined around the impact zone from a minimum mesh seed of 5 mm increasing to 40 mm. The foam core had 8 elements through the thickness giving a total of 44,860 C3D8R elements in the local region. 4786 S4R shell elements increasing from 40 mm to 550 mm were used in the global region. Therefore, the total element count for the hull was 49,646. All LVI/CAI simulations were completed using ABAQUS/Explicit on the Kelvin-2 Northern Ireland High Performance Computing (NI-HPC) Linux cluster with 20 CPUs. The run time of these hull models was approximately 9-10 hours.

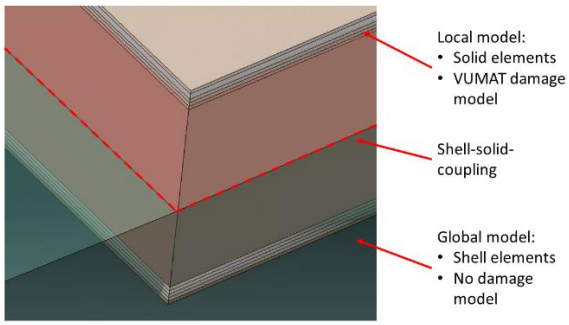

Figure 4: Detailed view of the global-local region of the hull.

3 RESULTS

3.1 eFoil impact results

Figure 5 shows the force-time and kinetic energy results for the local eFoil model after impact with rigid and ice projectiles. It can be seen that the 5 m/s (2kg) rigid impact produces the typical impact profile with a peak force of 6.7 kN. The peak force on the structure was 8 kN when impacted with an ice impactor (1 kg) at 17.5 m/s. In this case, because the ice block fails catastrophically, the time of the impact event is around half of the rigid body impact.

Looking at the energy absorption, from the kinetic energy plots in Figure 5b, the absorbed energy for the 5 m/s rigid impactor was 10.4 J. Looking at the higher velocity ice impacts (17.5 m/s), the absorbed energy during the 0.05 kg impact was 6.5 J, 84% of the original kinetic energy. The absorbed energy during the 1 kg impact was 73.5 J, 48% of the original kinetic energy.

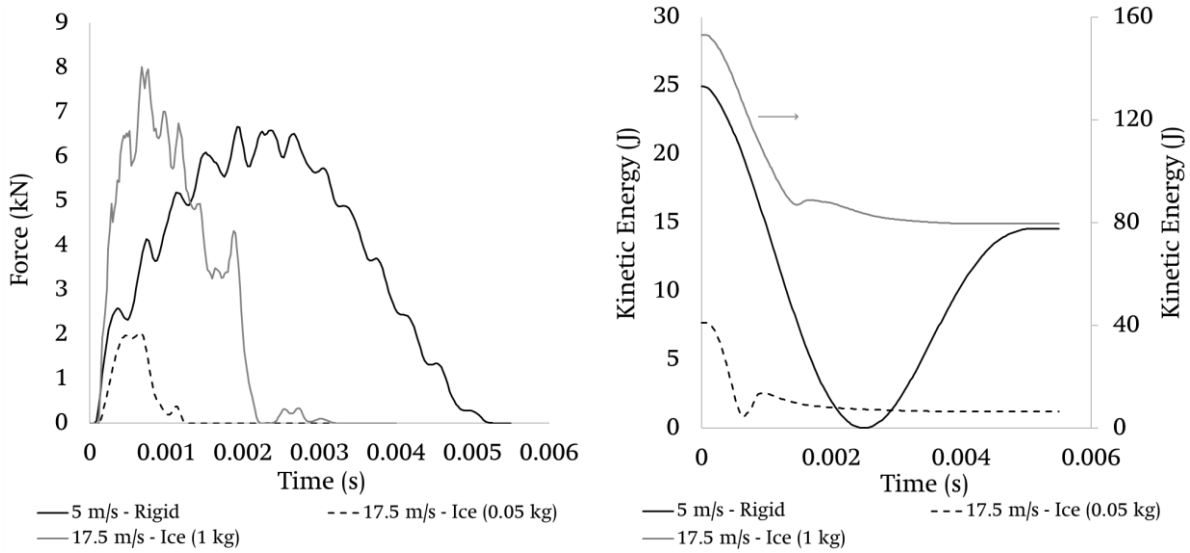

a) Force-time plots b) Kinetic energy plots

Figure 5: Force-time and kinetic energy results for the local eFoil model.

Figure 6 shows the spalling and splitting profile of ice on impact with the leading edge at 17 m/s. Delamination in these cases was negligible when compared with the rigid body impact.

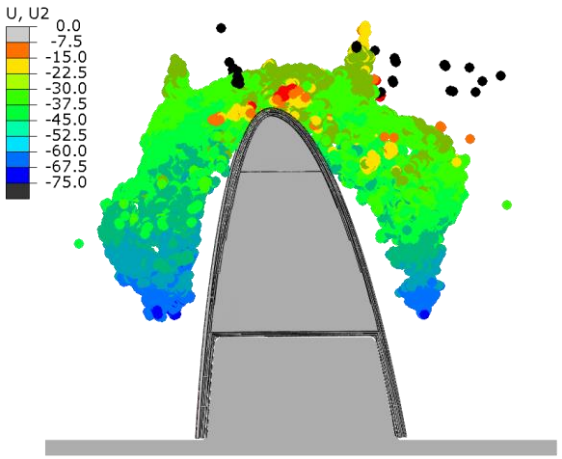

Figure 6: Spalling and splitting profile of ice on impact with the leading edge at 17 m/s.

Figure 7 compares the interlaminar delamination and intralaminar matrix damage produced on both the local and global-local models following a 25J impact with a rigid projectile. It can be seen that both models predict similar damage patterns for both measures with some variation in local magnitude.

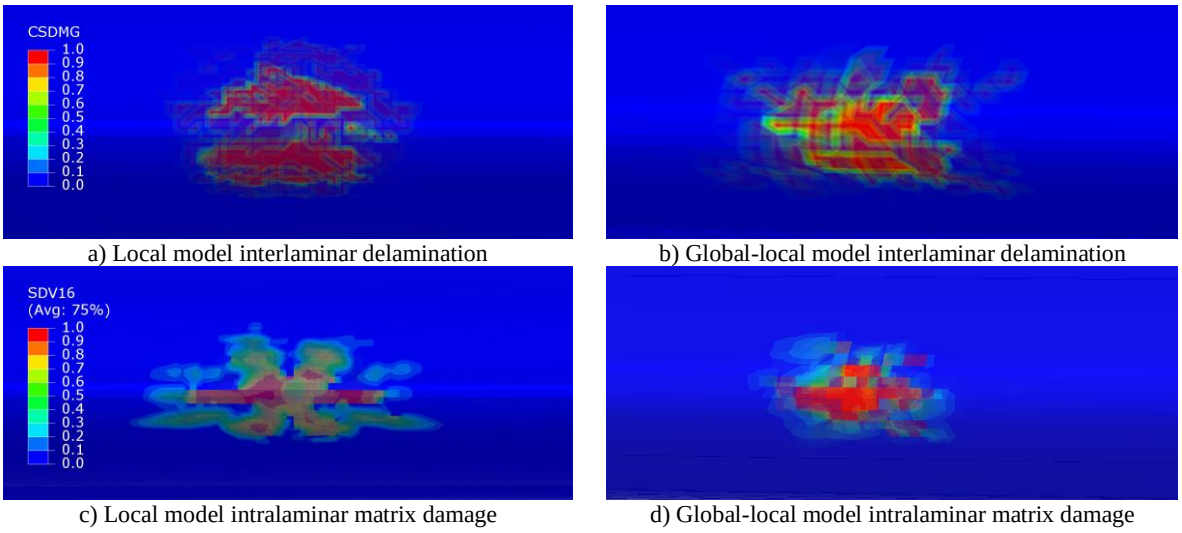

a) Local model interlaminar delamination

b) Global-local model interlaminar delamination

c) Local model intralaminar matrix damage

d) Global-local model intralaminar matrix damage

Figure 7: Comparison of mesoscale and global-local model damage predictions

The runtime for the local model was 2.5 hrs while the global-local model had a runtime of 3.5 hrs. It has been shown that when the volume of the eFoil structural analysis increased by twenty-five times and the total number of elements increased by 56% the run time increased by 40%.

3.2 Hull impact results

Figure 8 shows the predicted force-time and CAI residual strength plots for the flat hull model after the 10 knot (5 m/s) impact. The peak force in this case was 6.2 kN. Figure 8b shows that the CAI strength reduced from 522 MPa without impact damage to 258 MPa with impact damage.

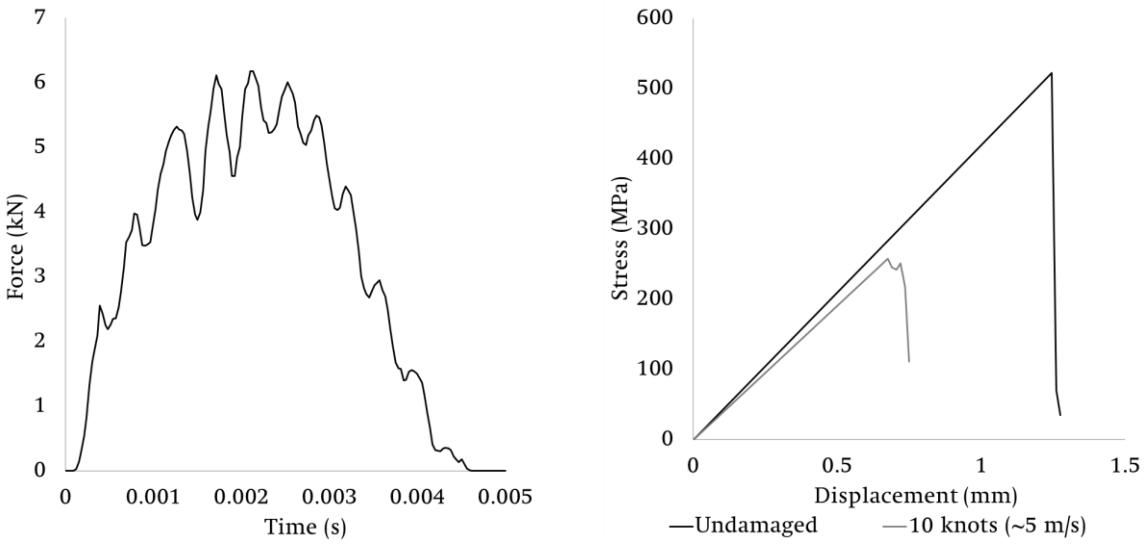

a) Force-time plot

b) CAI residual strength plots

Figure 8: Force-time and CAI results for flat hull model at different impact velocities.

Figure 9 shows the predicted matrix damage after a 2 kg rigid body, 10 knot impact on the global-

local model of the hull. In this case, interlaminar delamination was negligible and the permanent indentation on the surface of the hull was approximately 6 mm. No rupture occurred but the approximate area of intralaminar matrix damage was 690 mm^2. Approximately 66% of the initial kinetic energy of this impact was absorbed by the hull structure.

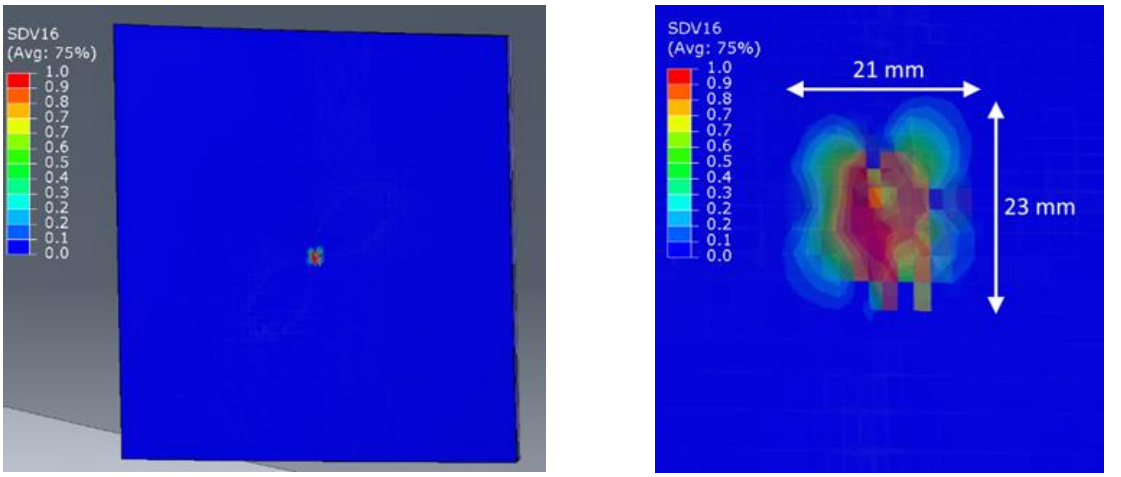

a) Matrix damage in global-local regions

b) Detailed view of matrix damage in local region

Figure 9: Post impact matrix damage profiles on the global-local hull model.

5 CONCLUSIONS

The work completed herein has developed a number of representative models to understand the susceptibility of eFoil propulsion systems and composite hull structures to in-service damage. A series of local (mesoscale) and global-local (multi-scale) models have been developed to predict the effects of damage either locally or on the entire structure.

It has been shown that these eFoil structures can resist impact with small ice blocks, even at the peak vessel velocity of 17.5 m/s. For example, when struck by a 0.05 kg ice block, the eFoil successfully split the block of ice on impact with minimal damage to the structure.

Damage to the hull structure has also been predicted. When the hull section was modelled as a flat panel, a 2 kg impactor with an equivalent impact velocity of 10 knots was rebounded after producing both delamination and matrix damage. 50% of the compressive strength of the specimen was retained post-impact. For the global-local model, the permanent indentation on the surface of the hull was approximately 6 mm.

The models herein have demonstrated the impact resistance of different maritime structures when exposed to likely impact events from their operating environment. Future work will refine these models further to improve prediction accuracy and consider other types of marine debris.

ACKNOWLEDGEMENTS

This study was conducted within the Belfast Maritime Consortium UKRI Strength in Places project, ‘Decarbonisation of Maritime Transportation: A return to Commercial Sailing’ led by Artemis Technologies, Project no. 107138.

REFERENCES

[1] International Maritime Organization (IMO). Initial IMO GHG Strategy 2019. https://www.imo.org/en/MediaCentre/HotTopics/Pages/Reducing-greenhouse-gas-emissions-from-ships.aspx.

[2] Horel B. System-based modelling of a foiling catamaran. Ocean Eng 2019;171:108–19. https://doi.org/10.1016/j.oceaneng.2018.10.046.

[3] Tan W, Falzon BG, Chiu LNS, Price M. Predicting low velocity impact damage and Compression-After-Impact (CAI) behaviour of composite laminates. Compos Part A Appl Sci Manuf 2015;71:212–26. https://doi.org/10.1016/j.compositesa.2015.01.025.

[4] McQuien JS, Hoos KH, Ferguson LA, Iarve E V., Mollenhauer DH. Geometrically nonlinear regularized extended finite element analysis of compression after impact in composite laminates. Compos Part A Appl Sci Manuf 2020;134. https://doi.org/10.1016/j.compositesa.2020.105907.

[5] Falcó O, Lopes CS, Sommer DE, Thomson D, Ávila RL, Tijs BHAH. Experimental analysis and simulation of low-velocity impact damage of composite laminates. Compos Struct 2022;287:115278. https://doi.org/10.1016/j.compstruct.2022.115278.

[6] Sun XC, Hallett SR. Failure mechanisms and damage evolution of laminated composites under compression after impact (CAI): Experimental and numerical study. Compos Part A Appl Sci Manuf 2018;104:41–59. https://doi.org/10.1016/j.compositesa.2017.10.026.

[7] Yu Z, Lu W, van den Berg M, Amdahl J, Løset S. Glacial ice impacts: Part II: Damage assessment and ice-structure interactions in accidental limit states (ALS). Mar Struct 2021;75. https://doi.org/10.1016/j.marstruc.2020.102889.

[8] Sun J, Huang Y. Investigations on the ship-ice impact: Part 1. Experimental methodologies. Mar Struct 2020;72:1–29. https://doi.org/10.1016/j.marstruc.2020.102772.

[9] Ringsberg JW, Heggelund SE, Lara P, Jang B-S, Hirdaris SE. Structural response analysis of slamming impact on free fall lifeboats. Mar Struct 2017;54:112–26. https://doi.org/10.1016/j.marstruc.2017.03.004.

[10] Cheng ZQ, Tan W, Xiong JJ. Modelling pre-fatigue, low-velocity impact and post-impact fatigue behaviours of composite helicopter tail structures under multipoint coordinated loading spectrum. Thin-Walled Struct 2022;176. https://doi.org/10.1016/j.tws.2022.109349.

[11] Nagaraj MH, Carrera E, Petrolo M. A global-local approach to the high-fidelity impact analysis of composite structures based on node-dependent kinematics. Compos Struct 2023;304:116307. https://doi.org/10.1016/j.compstruct.2022.116307.

[12] Nagaraj MH, Petrolo M, Carrera E. A global-local approach for progressive damage analysis of fiber-reinforced composite laminates. Thin-Walled Struct 2021;169:108343. https://doi.org/10.1016/j.tws.2021.108343.

[13] Montemurro M, Fiordilino GA, Carrera E. Multi-level optimisation of composite structures through a global-local modelling approach based on high-order theories. Comput Struct 2023;275:106932. https://doi.org/10.1016/j.compstruc.2022.106932.

[14] Reinoso J, Blázquez A, Estefani A, París F, Cañas J, Arévalo E, et al. Experimental and three-dimensional global-local finite element analysis of a composite component including degradation process at the interfaces. Compos Part B Eng 2012;43:1929–42. https://doi.org/10.1016/j.compositesb.2012.02.010.

[15] Ferraiuolo M, Palumbo C, Sellitto A, Riccio A. Global/local finite element analyses supporting the design of a ceramic matrix composite wing leading edge of a re-entry vehicle. Mater Today Proc 2021;34:31–5. https://doi.org/10.1016/j.matpr.2019.12.124.

[16] ABAQUS 2016 Documentation. ABAQUS Theory Manual. 2017.

[17] Faggiani A, Falzon BG. Predicting low-velocity impact damage on a stiffened composite panel.

Compos Part A Appl Sci Manuf 2010;41:737–49. https://doi.org/10.1016/j.compositesa.2010.02.005.

[18] Falzon BG, Apruzzese P. Numerical analysis of intralaminar failure mechanisms in composite structures. Part I: FE implementation. Compos Struct 2011;93:1039–46. https://doi.org/10.1016/j.compstruct.2010.06.028.

[19] Tan W, Falzon BG. Modelling the crush behaviour of thermoplastic composites. Compos Sci Technol 2016;134:57–71. https://doi.org/10.1016/j.compscitech.2016.07.015.

[20] Tan W, Falzon BG, Price M. Predicting the crushing behaviour of composite material using high-fidelity finite element modelling. Int J Crashworthiness 2015;20:60–77. https://doi.org/10.1080/13588265.2014.972122.

[21] Varandas LF, Catalanotti G, Melro AR, Falzon BG. On the importance of nesting considerations for accurate computational damage modelling in 2D woven composite materials. Comput Mater Sci 2020;172. https://doi.org/10.1016/j.commatsci.2019.109323.

[22] Chiu LNS, Falzon BG, Boman R. A continuum damage mechanics model for the analysis of the crashworthiness of composite structures: a work in progress. Proc. 15th Aust. Aeronaut. Conf., Melbourne, Australia: 2013.

[23] Tan W, Falzon BG. Modelling the nonlinear behaviour and fracture process of AS4/PEKK thermoplastic composite under shear loading. Compos Sci Technol 2016;126:60–77. https://doi.org/10.1016/j.compscitech.2016.02.008.

[24] Catalanotti G, Camanho PP, Marques AT. Three-dimensional failure criteria for fiber-reinforced laminates. Compos Struct 2013;95:63–79. https://doi.org/10.1016/j.compstruct.2012.07.016.

[25] Daniel IM, Luo J-J, Schubel PM. Three-dimensional characterization of textile composites. Compos Part B Eng 2008;39:13–9. https://doi.org/https://doi.org/10.1016/j.compositesb.2007.02.002.

[26] AITM Airbus Test Method. Fiber Reinforced plastics determination of compression strength after impact. 2010.

[27] Liu K, Liu JL, Wang Z. A damage threshold prediction model of CFRP panel by hail impact based on delamination mechanism. Eng Fract Mech 2020;239. https://doi.org/10.1016/j.engfracmech.2020.107282.

[28] Gingold RA, Monaghan JJ. Smoothed particle hydrodynamics: theory and application to non-spherical stars. Mon Not R Astron Soc 1977;181:375–89. https://doi.org/10.1093/mnras/181.3.375.

[29] Arezoo S, Tagarielli VL, Petrinic N, Reed JM. The mechanical response of Rohacell foams at different length scales. J Mater Sci 2011;46:6863–70. https://doi.org/10.1007/s10853-011-5649-7.